International Journal of Computer Assisted Radiology and Surgery (2018) 13:637–646
https://doi.org/10.1007/s11548-018-1712-z

ORIGINAL ARTICLE

Planning nonlinear access paths for temporal bone surgery

Johannes Fauser[1] · **Georgios Sakas**[1] · **Anirban Mukhopadhyay**[1]

Received: 30 January 2018 / Accepted: 16 February 2018 / Published online: 3 March 2018

Abstract

Purpose Interventions at the otobasis operate in the narrow region of the temporal bone where several highly sensitive organs define obstacles with minimal clearance for surgical instruments. Nonlinear trajectories for potential minimally invasive interventions can provide larger distances to risk structures and optimized orientations of surgical instruments, thus improving clinical outcomes when compared to existing linear approaches. In this paper, we present fast and accurate planning methods for such nonlinear access paths.

Methods We define a specific motion planning problem in $\mathrm{SE}(3) = \mathbb{R}^3 \times \mathrm{SO}(3)$ with notable constraints in computation time and goal pose that reflect the requirements of temporal bone surgery. We then present κ-RRT-Connect: two suitable motion planners based on bidirectional Rapidly exploring Random Tree (RRT) to solve this problem efficiently.

Results The benefits of κ-RRT-Connect are demonstrated on real CT data of patients. Their general performance is shown on a large set of realistic synthetic anatomies. We also show that these new algorithms outperform state-of-the-art methods based on circular arcs or Bézier–Splines when applied to this specific problem.

Conclusion With this work, we demonstrate that preoperative and intra-operative planning of nonlinear access paths is possible for minimally invasive surgeries at the otobasis.

Keywords Minimally invasive · Temporal bone surgery · Statistical shape models · Nonholonomic motion planning · Curvature constraint · RRT

Introduction

In the last decades, more and more minimally invasive procedures are introduced in the clinical work place [2]. At the otobasis, the focus of research has been the drilling of either a single [12,20] or multiple [25] linear access paths through the temporal bone to the cochlea and initial reports on clinical studies have been presented [4,17]. In such interventions, several obstacles or risk structures, e.g., the facial nerve and its small branch (Fig. 1, yellow objects), severely limit the space that is available for drilling.

Unlike these linear approaches, nonlinear drilling provides several potential advantages: larger distances to risk structures, correcting misalignments while drilling, and optimization of orientation at the goal point (e.g., for the insertion of the electrode during a cochlear implantation or for instrument alignment). Yet, nonlinear planning at the otobasis is difficult to deploy due to the limited space and time constraints on intra-interventional planning. To the best of our knowledge, such an approach has never been investigated. In this paper, we consider the use of a curvature constrained drilling unit and propose two new RRT-Connect [18] algorithms to quickly (re-)compute feasible access paths for said robot: once at the beginning of the intervention and regularly in between if navigation errors occur (Fig. 1).

In recent years, significant progress has been made in the development of continuum robots and instruments for minimally invasive medical applications [3]. Many of these can be categorized as "curvature constrained objects." These include, for example, steerable needles [6,7] for interventions in soft tissue [8,21] or flexible endoscopes [10]. If such underactuated systems are used, where instrument steering is limited to certain directions, nonholonomic motion planning based on the Rapidly Exploring Random Tree [1,18] or even optimal randomized motion planners [11,15] are used to

Electronic supplementary material The online version of this article (https://doi.org/10.1007/s11548-018-1712-z) contains supplementary material, which is available to authorized users.

✉ Johannes Fauser
johannes.fauser@gris.tu-darmstadt.de

[1] Department of Computer Science, Technische Universität Darmstadt, Darmstadt, Germany

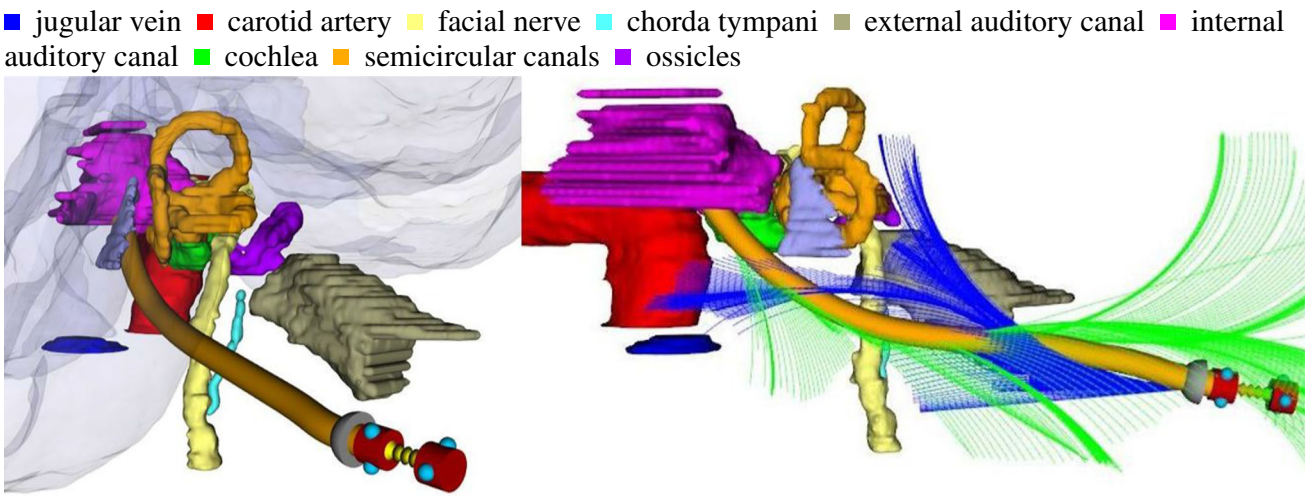

Fig. 1 A nonlinear access path (orange) has to be drilled through the temporal bone (empty space) by a surgical robot (colored) to reach the target of an intervention. Various organs (different colors) form obstacles that our planning algorithms have to avoid (e.g., blue and green search graph of a RRT-Connect)

plan feasible trajectories around obstacles for the underlying instrument.

In medical applications, the main focus mainly lies on steerable needles where planning is done with variants of the RRT. These methods consider, for example, special distance functions [21] or the reachable set of the nearest states [24]. Other methods speed up the convergence via potential fields [29] or utilize heavy parallelization [19].

The planning of trajectories for (unmanned) aerial vehicles such as drones or missiles also requires curvature constrained motion planning. Here, the development of an analytical solution of the 3D Dubins Problem [14] leads to an RRT*-solver [22] in the case that start and goal regions are sufficiently far away. Moreover, Yang et al. [27,28] presented an RRT* with Bézier splines as local planning technique.

However, curvature constrained motion planning for temporal bone surgery requires fast and precise algorithms with start and goal regions in SE(3) within a small and dense environment. Although we were able to show the general feasibility of such trajectories within the otobasis [9], a reliable method does not yet exist.

The main contribution in this paper is then twofold: First of all, we present two RRT-Connect algorithms which achieve fast path planning for nonlinear temporal bone surgery. Secondly, we address a novel evaluation strategy in case of limited annotated data sets: The robustness of such planners is shown on synthetic anatomies based on statistical shape models from real CT patient data.

Objective

Minimally invasive procedures require a planning step that computes feasible trajectories while respecting potential constraints such as clearance to organs or instrument mobility. After the computation of a set of solutions, these are then optimized according to a cost function or other optimization strategies [13,25].

In motion planning, relevant parameters are usually expressed in a specific Problem Formulation [18]. In this section, we describe the details for temporal bone surgery and how they are incorporated in the following Formulation:

Problem Formulation For Temporal Bone Surgery

1. Let $O \subset \mathrm{SE}(3) = \mathbb{R}^3 \times \mathrm{SO}(3)$ be the obstacle region, defined by the location of several risk structures $\{\mathscr{R}\}_i \subset \mathbb{R}^3, 0 \leq i \leq N$. That is, $O := \{q = (x,h) \in \mathrm{SE}(3) | \exists i, 0 \leq i \leq N : x \in \mathscr{R}_i\}$. Let $C_{\text{free}} = \{q \in \mathrm{SE}(3) | q \notin O\}$ be the free space of the configuration space.
2. Let $C_I \subset C_{\text{free}}$ be the initial region.
3. Let $M_G \subset C_{\text{free}}$ be a set of states. The goal region C_G is then defined as

$$C_G \equiv C_G(\varepsilon_G, \phi_G) = \{q(x,h) \in \mathrm{SE}(3) \mid \|x - y\|_{\mathbb{R}^3} < \varepsilon_G, \rho(h,g) < \phi_G, \text{ for a } \hat{q}(y,g) \in M_G\},$$

where ρ is defined as in Eq. (1) and

(i) $\varepsilon_G \in \mathbb{R}^+$ is the maximally allowed Euclidean distance and
(ii) $\phi_G \in [0, \pi]$ is the maximally allowed angular difference at a specific goal state.

4. Let $d_{\max} \in \mathbb{R}^{0+}$ be the safety distance to risk structures. Let $r_d \in \mathbb{R}^+$ be the radius and $\kappa_{\max} \in \mathbb{R}^+$ the maximum curvature constraint of the drilling robot.

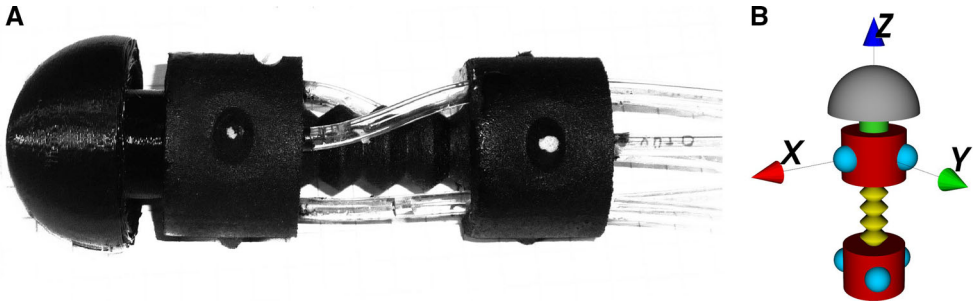

Fig. 2 **a** Prototype of the hydraulically driven robot with a drill bit at the front. **b** Model of the robot based on geometric primitives and its local coordinate frame

5. Let $T_{\max} \in \mathbb{R}^+$ be the maximum time constraint available for planning.
6. Task: Find a path $\gamma(t) : [0, 1] \to \mathrm{SE}(3)$ satisfying

   (i) $\gamma(0) \in C_I$
   (ii) $\gamma(1) \in C_G$
   (iii) $\forall t \in (0, 1) : \left\|\gamma''(t)\right\| < \kappa_{\max}$
   (iv) $\forall t \in [0, 1], o \in O : \|\gamma(t) - o\|_{\mathbb{R}^3} > r_d + d_{\max}$

   or report that no path could be found in the available time $T_{\max}$.

Item 1 of this Problem Formulation introduces obstacles in $\mathbb{R}^3$ (e.g., the facial nerve) that have to be circumnavigated, as well as the free space, which defines potential positions the drilling unit can occupy. *Item 2* corresponds to potential positions at the skull's surface that serve as entry points of instruments, whereas *Item 3* defines a spherical volume in $\mathbb{R}^3$ as the intervention's target together with a threshold ϕ_G that limits the potential orientation within this target volume. The orientation between two configurations is compared in the quaternion metric (see e.g., [18])

$$\begin{aligned} \rho(h_1, h_2) &= \min\{\rho_S(h_1, h_2), \quad \rho_s(h_1, -h_2)\} \\ \rho_s(h_1, h_2) &= \cos^{-1}(a_1a_2 + b_1b_2 + c_1c_2 + d_1d_2). \end{aligned} \tag{1}$$

In this paper, we consider the use of a prototype robot (Fig. 2) currently under development for the creation of nonlinear access paths. If we consider the z-axis in the local coordinate frame of the model as the robot's *line of view*, we want to match its pose with the ones at start and goal states: Initial states should be close to the skull's surface normal in order to minimize deviation from the desired trajectory due to forces applied during drilling. For a cochlear implantation, for example, goal states at the round window would represent the optimal insertion angle. Here, work has been done to limit the deviation from the optimum to less than 5° [26].

The robot's limitations are then included via *Item 4*: The radius of the drill bit and an additional safety distance to account for navigation errors or heat generation are combined to a distance constraint. Additionally, the maximum turning angle of the prototype results in a curvature constraint. *Item 5:* Potential misalignments during navigation require an intra-interventional replanning step to either provide a new corrected trajectory or stop the drilling. Therefore, an algorithm has to be fast enough to provide a smooth intervention. *Item 6:* A motion planning algorithm for this procedure will then try to find a feasible path in the available time which would result in a trajectory connecting both a start and a goal state (i, ii), observing a maximally allowed curvature (iii) and last, a necessary distance to risk structures (iv).

Note 1 This formulation remains valid in the case of replanning where the initial region C_I of Item 2 will be set to the current pose of the robot.

Note 2 This formulation extends the problem of trajectory planning in soft tissue for bevel-tip needles, where alignment of instruments [23] and regular fast replanning [21] is needed, by introducing constraints on both start and goal orientations. We expect our planners to be useful for this kind of application as well.

Methods

The main difficulty of this problem is the fast and precise matching of the goal's pose. An intuitive way to address this problem is to use an RRT-Connect algorithm [16]. This method, unlike basic RRTs, grows search trees from both the goal and the initial region in an attempt to connect these two. With this strategy, more possible connections are available than just those between search tree and goal regions. Thus, successfully finding an access path is more likely. The general RRT-Connect can be described as follows (Algorithm 1):

Two trees $\mathcal{T}_I$, $\mathcal{T}_G$ are initialized with states of the initial and the goal region, respectively. Both trees are iteratively extended until either the maximally allowed time $T_{\max}$ is reached or the graphs are connected successfully. In each iteration, the two search trees take turn in the following procedure: A random state is drawn from the free space C_{free}. Then, the nearest neighbors to the current tree are computed according to a previously defined distance function. For each

of these configurations, the local steering function computes an expansion toward the random state. If no collision with obstacles occurs along this path, the state is added to the tree. Last, the algorithm tries to connect both trees according to the state space's constraints (in our case the path needs to be two times continuously differentiable). If both trees are connected within the given time threshold $T_{\max}$, the resulting path is returned. Otherwise, failure is reported.

Algorithm 1 κ-RRT-Connect

1: $\mathcal{T}_I \leftarrow$ initial_states()
2: $\mathcal{T}_G \leftarrow$ goal_states()
3: **while** time_spend() $< T_{max}$ and $not\_connected(\mathcal{T}_I, \mathcal{T}_G)$ **do**
4: $q_{rand} \leftarrow$ sample_state(C_{free})
5: $\mathcal{T} \leftarrow$ alternate($\mathcal{T}_I, \mathcal{T}_G$)
6: $\{q\}_k \leftarrow$ k_nearest_neighbors($\mathcal{T}, q_{rand}$)
7: **for all** q_{near} in $\{q\}_k$ **do**
8: $q_{next} \leftarrow$ steer($q_{near}, q_{rand}, \Delta t$)
9: **if** collision_free(q_{near}, q_{next}) **then**
10: extend_tree($\mathcal{T}, q_{near}, q_{next}$)
11: **end for**
12: attempt_connection($\mathcal{T}_I, \mathcal{T}_G$)
13: **end while**

In the following, we shortly recall two local steering methods, one based on circular arcs of varying curvature and one based on Bézier–Splines. We then present two individual solutions that extend these planners to RRT-Connect versions.

Bevel-Tip-RRT & k-B-RRT-Connect: We use the local steering function developed for Bevel-tip needles presented in [21] to create access paths of variable curvature. This method extends the search tree along circular arcs of variable radii. The RRT-Connect version uses Dubins Paths in 3D to connect the search trees as, unlike circular arcs, this is a technique to connect states in SE(3).

Spline-Based-RRT & k-SB-RRT-Connect: The second RRT utilizes cubic Bézier–Splines to interpolate in SE(3), resulting in an approximation of states in the search tree and a two times continuously differentiable trajectory [28]. Here, the local steering method can be used naturally to attempt a connection.

The individual steps in Algorithm 1 (lines 4, 6, 8, 12) are then as follows:

sample_state: Sampling in SE(3) would require solving a two point boundary value problem, i.e., matching both location and orientation at the random state. This is not possible with either steering function. Instead, a state is merely sampled in $\mathbb{R}^3$, and the direction is implicitly defined according to the respective method.

k_nearest_neighbors: The nearest neighbor function and its underlying metric have significant impact on the time efficiency and the theoretical properties of the algorithm. For curvature constrained instruments, the Euclidean metric does not represent a good approximation on the actual distance. On the other hand, the computation of a more complex metric like the reachable set of a particular state [24] can be very time consuming. As the main interest in this application lies in the fast computation of a feasible path, we return the k-nearest neighbors in terms of the efficiently computable metric

$$d(q_1(x,h_1),q_2(y,h_2)) : \mathrm{SE}(3)\times\mathrm{SE}(3)\rightarrow\mathbb{R}^3 := \|x-y\|_{\mathbb{R}^3}+\rho(h_1,h_2)$$

steer: κ-B-RRT-Connect propagates the search along states on circular arcs. The local planner of κ-SB-RRT-Connect uses a spline consisting of two Bézier–Spirals to expand the search tree. We refer to the original papers [21] and [28] for a detailed description.

attempt_connection: The original RRT-Connect does not address nonholonomic planning and considers the trees connected if both trees meet at the random sample. This approach would result in a discontinuous orientation at the connecting state as we sample only in $\mathbb{R}^3$ and do not enforce a specific orientation. Instead, a two point boundary value problem has to be solved in our approach to match both position and orientation:

First, we search for a state of the other tree in the vicinity of q_{next}. Specifically, we check if a state lies within a cone that apex and direction are described by the location and orientation of q_{next}. If such a state is found, we try to connect these two:

The κ-B-RRT-Connect algorithm connects two corresponding states by solving the 3D Dubins problem with the geometric approach presented in [14]. A similar method is used in [22]. Both papers address the computational complexity of their approach. However, our c++ implementation requires on average only 45 microseconds to solve the underlying nonlinear system of equations which makes it suitable for fast computation.

The κ-SB-RRT-Connect algorithm iteratively uses the local steering function to steer from q_{next} to its counterpart and vice versa. This procedure is repeated until either the interpolation criterion of the Bézier–Spline is satisfied during an iteration or the states missed each other, and thus no connection was possible.

Scenarios for the temporal bone

We address three typical medical interventions for the experiments to show the general suitability for temporal bone surgery (Fig. 3): one access to the cochlea via the facial recess

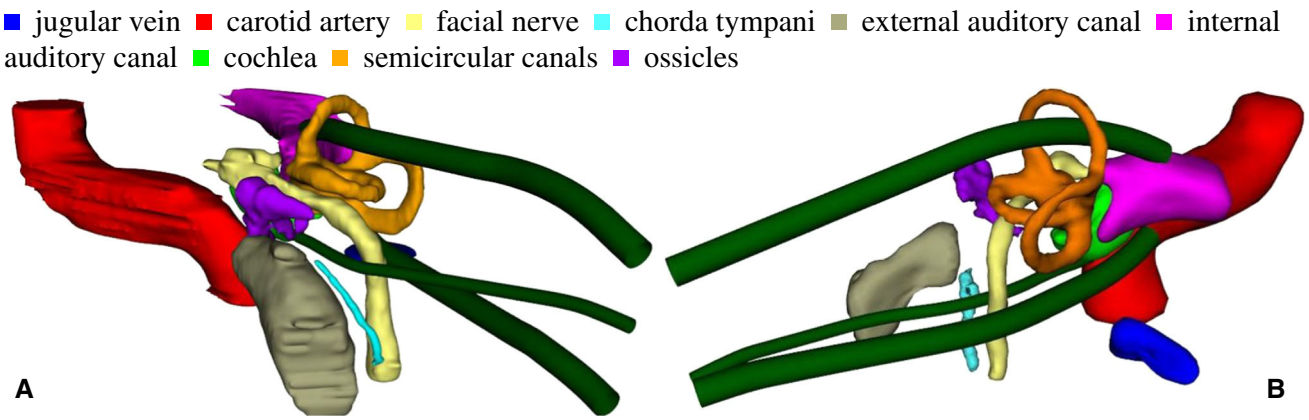

Fig. 3 Examples of the access paths (Cochlea-/SSC-/RL-Access) for real (**a**) and synthetic (**b**) anatomies

(Cochlea-Access) and two accesses to the internal auditory canal: through the superior semicircular canal (SSC-Access) and via the retro-labyrinthine region (RL-Access). Parameters for each Problem Formulation (see "Objective" section) are listed in Table 1. The curvature constraint reflects our current robot prototype. We tested with higher values of r_d and $d_{\max}$ for the RL- and SSC-Access as there is usually more space between obstacles. The time and orientation constraints were chosen according to real applications [23,26].

The risk structures, i.e., organs in the vicinity of access paths that must not be harmed, were extracted from real CT data of patients. To this purpose, our clinical partners manually segmented the internal carotid artery and jugular vein bulb, facial nerve and chorda tympani, cochlea, ossicles and labyrinth as well as the internal and external auditory canal in 40 high quality, but typical routine CT scans of the human temporal bone (Siemens Somatom, average resolution $0.18 \times 0.18 \times 0.4\,\text{mm}^3$).

The manual assembly of such real scenarios is a necessary but extremely laborious and time consuming task. However, a statistical analysis of the motion planner's performance requires a much larger number of samples than this manual procedure can provide. Consequently, we divided the experiments into two setups:

Real anatomies: For the first 22 data sets, we also segmented the brain and the skull's surface. In the resulting 3D environment, entry and target positions of potential interventions were manually placed in each individual data set with the help of a custom planning tool to provide samples on real patients (Fig. 3a).

Synthetic anatomies: First, we created statistical shape models [5] of the manually segmented risk structures of the otobasis in all 40 data sets. Then, we generated 100 synthetic anatomies based on the real ones. For each new synthetic anatomy, one of the real anatomies was chosen randomly to serve as an atlas, including its risk structures and its goal regions of the three potential interventions. A variation of the statistical shape models was then registered to the atlas to replace each original structure with an altered variant (Fig. 3b).

Experiments

In the following, we describe in detail the setup of real and synthetic anatomies as well as the parameters of our motion planners.

Real anatomies: In each data set and for each of the three applications (RL-, SSC-, Cochlea-Access), we placed one state within the temporal bone and one state on the skull's surface to define the regions C_I and C_G of the Problem Formulations. Start states were positioned at the bottom of the internal auditory canal, at its top and next to the round window for the RL-, SSC- and Cochlea-Access, respectively. This resembles a potential position of an acoustic neuroma (RL-, SSC-Access) or the entry point of the electrode in a

Table 1 Parameters for the problem formulations (see "objective" section) of the three access paths

	$\kappa_{\max}$	ε_G	ϕ_G (deg)	$d_{\max}$ (mm)	r_d (mm)	$T_{\max}$ (s)
Cochlea-Access	0.05	1.0	5	0.3	0.5	0.5
SSC-Access	0.05	1.0	5	0.5	1.0	0.5
RL-Access	0.05	1.0	5	1.0	1.0	0.5

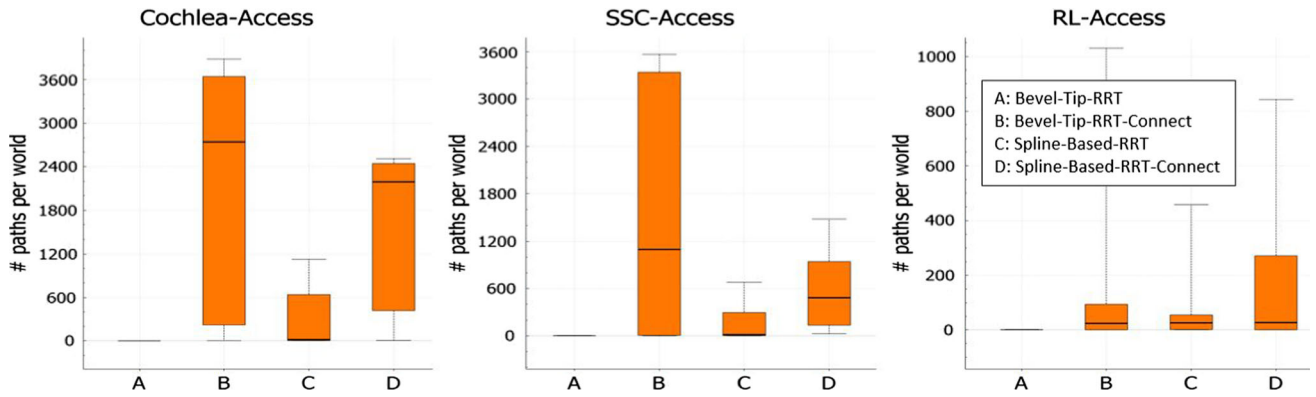

Fig. 4 Box plots for each access canal about the number of paths found by the individual planners in 22 real anatomies (higher = better)

Table 2 Performance of each planner for the real anatomies. Measured in median number of paths (#), median number of paths per second (#/s) and percentage of failed scenarios (F)

	Cochlea-Access			SSC-Access			RL-Access		
	#	#/s	*F* (%)	#	#/s	*F* (%)	#	#/s	*F* (%)
Bevel-tip (A)	0	0	80	1	0.05	50	0	0	75
Bevel-tip-connect (B)	**2635**	**131.75**	5	**760**	**38**	**0**	4	0.2	45
Spline-based (C)	17	0.85	5	14	0.7	5	9	0.45	**25**
Spline-based-connect (D)	2031	101.55	**0**	442	22.1	**0**	**17**	**0.85**	40

Minimum and maximum values are shown in bold

cochlear implant (Cochlea-Access). The directions at these start states were defined as a compromise between the respective organ's normal at this position and a direction toward the skull's surface. Last, three states were placed on the skull with orientations approximately orthogonal to its surface which serve as goal states for the individual access paths.

Synthetic anatomies: For each new synthetic anatomy, random variations of the individual statistical shape models' modes were computed by sampling the corresponding eigenvalues between ± 1.0 times of their standard deviation. The resulting model was then registered with the reference atlas. For the respective goal states, we used the ones in the atlas. The start states required a new strategy for positioning, as their original pose in the atlas might be invalid. Thus, new start states were placed above/below the center of mass of the internal auditory canal (SSC-/RL-Access) and below the center of mass of the cochlea (Cochlea-Access). For orientation, individual reference points $P_{\text{ref}} \in \mathbb{R}^3$ were computed: for the RL-Access slightly inferior to the lower side of the bounding box of the facial nerve; for the SSC-Access above the center of mass of the semicircular canals and for the Cochlea-Access in the center of mass of the chorda tympani. The start states were then oriented so that the z-axis of the local coordinate frame points to the respective reference point.

Motion planning: In both setups, we let each of the four planners of "Methods" section calculate as many paths as possible within 20 s for all three applications. We used the number of found paths to quantify the performance of each planner. In order to compare the quality of paths computed by each planner, we measured for each trajectory both the deviation at the goal state and the minimal distance to risk structures.

For goal biasing, we chose a value of 25%. The *attempt_connection* method of κ-RRT-Connect was most successful with parameters $h = 5.0\,\text{mm}$ and $\alpha = 20°$ for height and angle of the cone. A kd-Tree was used for collision checking between states and obstacles. All experiments were performed on a system with an Intel Core i5-6500 CPU @ 3.20 GHz and 32,0 GB RAM.

Results

We start with analyzing the motion planners' results on real anatomies. Then, we discuss their generalization on synthetic data.

Real anatomies: First, we look at the number of paths found in a specific time to ensure a planner is fast enough for intra-operative replanning [21]. Figure 4 and Table 2 show the statistical distributions: For both the Cochlea- and the SSC-Access, our RRT-Connect algorithms clearly outperformed standard RRT planners. In the case of the RL-Access, the Spline-Based-RRT showed similar performance but none of the three algorithms really stands out. The number of paths found per second and the low number of failures indicate

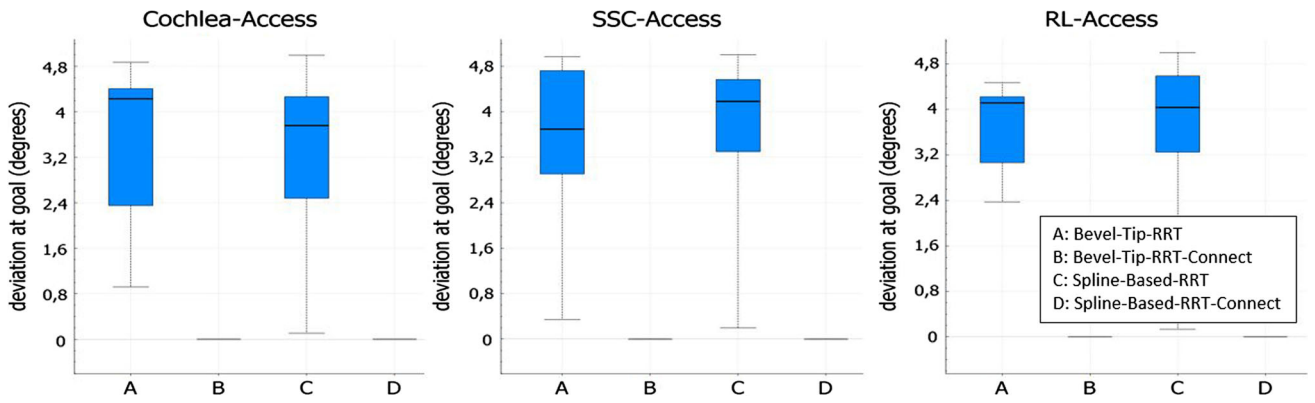

Fig. 5 Box plots about the deviation at the goal for the real anatomies (lower = better)

that κ-RRT-Connects work very well for the first two access canals, and we can expect that successful intra-operational planning can be performed in minimal time. In contrast, the search through the retro-labyrinthine region was unsuccessful for almost half of the anatomies. This is, however, not unexpected because the risk structures vary highly between patients: In case of a narrow passage between facial nerve and chorda tympani, a small semicircular canal or a high reaching bulb of the jugular vein, the creation of a feasible access path was impossible. Indeed, a careful inspection showed that in the 6 cases algorithm C failed and a high reaching jugular vein bulb made a trajectory of the requested size completely impossible. The discrepancy between the first two problem formulations and the latter is also due to the nature of relevant obstacles in the respective area. In the first two cases, a bottleneck had to be passed (two nerves/the SSC), whereas for the RL-Access the facial nerve and the jugular vein had to be circumnavigated.

Now we look at the matching of the goal's pose. Naturally, RRT-Connect algorithms matched the orientation of goal states perfectly, whereas the RRTs were limited to an approximation (Fig. 5). We also note that in all three cases both Bevel-Tip-RRT and Spline-Based-RRT tended to accomplish the maximal allowed deviation rather than a perfect match.

Next, we focus on the minimal distance an access path had to risk structures as this is usually the most relevant metric to clinicians. To this purpose, we interpolated between the states of the search tree at a resolution of 0.1 mm. For each of those interpolated states, we then sampled points on a circle with radius r_d and orthogonal to the state's direction and computed the minimal distance to the next obstacle. Figure 6 shows in small images the narrowest region that had to be passed together with three statistics for each planner across all 22 anatomies: the percentage how often it computed the best path for a specific anatomy (Best), the mean minimal distance its best path had to risk structures (Mean) and the overall best path it computed across all anatomies (Max). Clear superiority of a specific algorithm was not observable although the Spline-Based-RRT tended to find paths with the largest distance more often. Hence, our new κ-RRT-Connect did not suffer from lower quality. From the observed distances, we also got an impression of the average size of the passed bottleneck. This can help in the design for the robot prototype. According to Table 2, for example, κ-RRT-Connect always found trajectories for an SSC-Access with the specifications in Table 1, having on average still a minimal distance above 1.0 mm to the nearest obstacle.

Last we address the issue that in many scenarios the Spline-Based-RRT found paths with the highest minimal distance. A closer inspection showed that the κ-RRT-Connect just quickly found a solution as soon as the relevant obstacle had been passed. When we enlarged the allowed safety distance, the κ-RRT-Connect computed paths with similar minimal distances. Figure 7 shows an example of

A Bevel-Tip-RRT, **B** Bevel-Tip-RRT-Connect - **C** Spline-Based-RRT - **D** Spline-Based-RRT-Connect

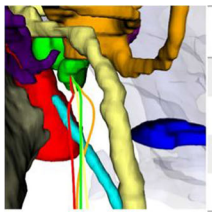

	Best (%)	Mean (mm)	Max (mm)
A	5.3	0.48	0.64
B	10.5	0.65	1.12
C	**42.1**	0.67	**1.32**
D	**42.1**	**0.68**	1.15

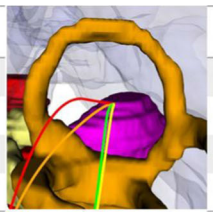

	Best (%)	Mean (mm)	Max (mm)
A	5.3	0.96	1.29
B	15.8	1.04	1.50
C	**42.1**	1.02	**1.63**
D	36.8	**1.13**	1.55

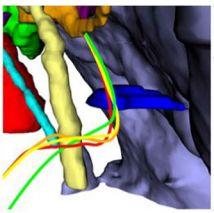

	Best (%)	Mean (mm)	Max (mm)
A	26	1.32	2.24
B	5.3	1.46	1.94
C	**57.9**	**1.66**	**2.35**
D	10.5	1.56	2.13

Fig. 6 Close-up of the narrowest region of each access canal. The corresponding table shows the mean and max distance of each planner over all real anatomies together with the percentage of how often each planner found the best path according to the maximum distance

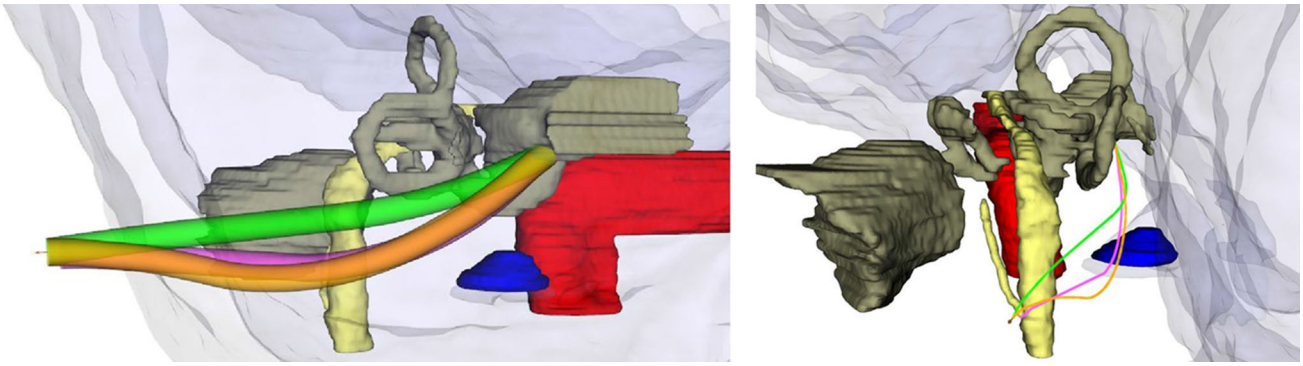

Fig. 7 RL-access planned by a standard RRT (pink tube) with safety distance 1.0 mm and by a κ-RRT-Connect (green, orange) with safety distances 1.0 and 1.5 mm, respectively

this behavior for the RL-Access with safety distance 1.0 and 1.5 mm.

Synthetic anatomies: To study the generalization of these specific cases, we then looked at synthetic scenarios. Instead of real anatomies we now worked with variances based on atlases of real data combined with the shape space of the statistical shape models. Our evaluations then included a much broader variety of anatomies. By randomly sampling the shape space, we also made sure that the individual real anatomies did not provide edge cases for the algorithms, a standard approach in motion planning [11,15].

The results in Figs. 8 and 9 and Table 3 show how the planners performed for each access canal. From the box plots, we can conclude that κ-RRT-Connect again tended to find many more paths. Their performances according to Table 3 supported the results of the real cases: For the given parameters of Table 1, access paths for the Cochlea- and SSC-Access were always possible, whereas for the RL-Access a high reaching jugular vein often prevented a feasible trajectory to be found. The number of paths found per second again indicated that bidirectional RRTs are suitable for intra-operational planning. An analysis of the orientation at the goal showed equivalent results to the real cases: RRTs hardly realize a good match of the desired orientation (Fig. 10). Although this was expected, it clearly supports our claim that bidirectional planners are required, if precise replanning is necessary.

Conclusion

In this paper, we address a minimally invasive procedure with demands on fast computation and high precision of both initial and goal pose. We present two suitable RRT-Connect motion planners, one based on Bézier–Splines, the other on circular arcs and 3D Dubins Paths, which quickly compute feasible curvature constrained access paths for the proposed interventions. The efficiency of these planners is shown in real CT data of patients as well as on randomized anatomies created from variations of statistical shape models. These tailored RRT-Connect algorithms outperform state-of-the-art one-directional planners and provide a reliable and fast method for planning access paths in temporal bone surgery.

In the future, we want to improve the approach for both methods with an optimization of planned paths regarding larger distances to risk structures or more advanced metrics. We also expect that an improvement of the connection

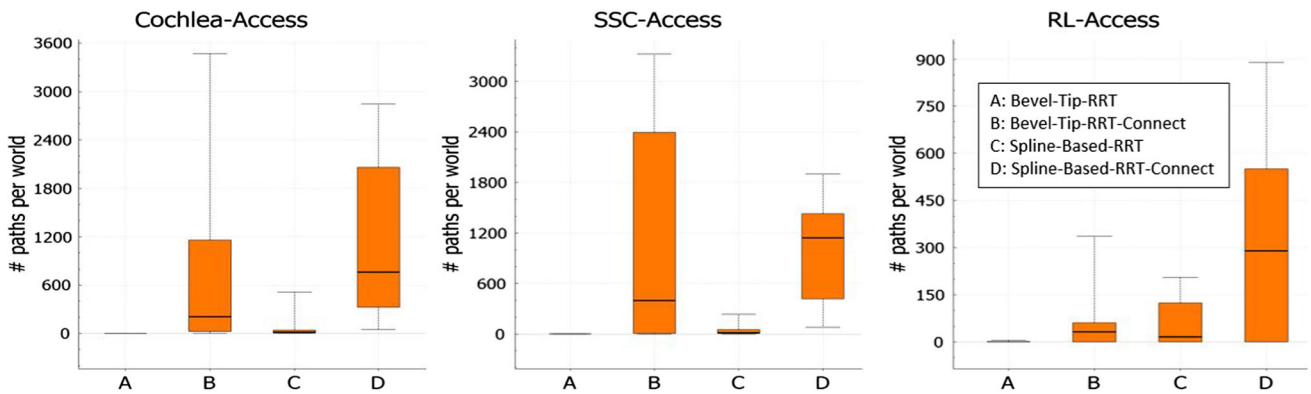

Fig. 8 Box plots about the success rates of the planners in 100 synthetic anatomies (higher = better)

Table 3 Measured in median number of paths (#), median number of paths per second (#/s) and percentage of failed scenarios (F)

	Cochlea-Access			SSC-Access			RL-Access		
	#	#/s	*F* (%)	#	#/s	*F* (%)	#	#/s	*F* (%)
Bevel-tip (A)	0	0	80	0	0	57	0	0	66
Bevel-tip-connect (B)	208	10.4	**0**	398	19.9	12	27	1.35	37
Spline-based (C)	15	0.75	7	14	0.7	7	15	0.75	**26**
Spline-based-connect (D)	**762**	**38.1**	**0**	**1144**	**57.2**	**0**	**273**	**13.65**	30

Minimum and maximum values are shown in bold

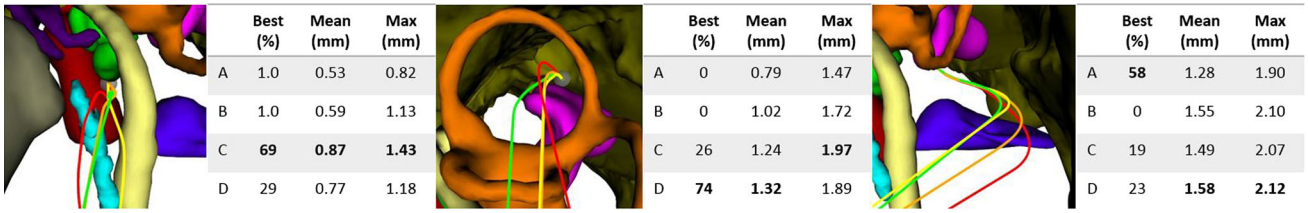

	Best (%)	Mean (mm)	Max (mm)
A	1.0	0.53	0.82
B	1.0	0.59	1.13
C	**69**	**0.87**	**1.43**
D	29	0.77	1.18

	Best (%)	Mean (mm)	Max (mm)
A	0	0.79	1.47
B	0	1.02	1.72
C	26	1.24	**1.97**
D	**74**	**1.32**	1.89

	Best (%)	Mean (mm)	Max (mm)
A	**58**	1.28	1.90
B	0	1.55	2.10
C	19	1.49	2.07
D	23	**1.58**	**2.12**

Fig. 9 Close-up of the narrowest region of each access canal. The corresponding table shows the mean and max distance of each planner over all synthetic anatomies together with the percentage of how often each planner found the best path according to the maximum distance

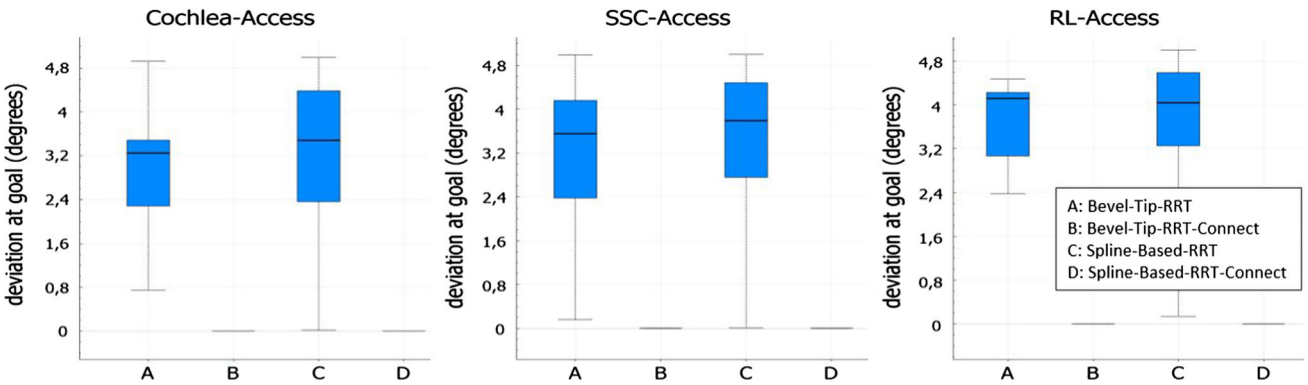

Fig. 10 Box plots about the deviation at the goal for 100 random synthetic anatomies (lower = better)

method of our RRT-Connects will result in better performances for difficult cases like passing the retro-labyrinthine region. Moreover, we would like to investigate the applicability of these general purpose planners for other medical interventions such as needle insertion in soft tissue [23] or flexible endoscopes [10]. We believe such precise nonlinear planning procedures are expected to be instrumental in improving interventions and advancing patient safety at operating rooms of the future.

Compliance with ethical standards

Funding The research Project MUKNO II is funded by the DFG.

Conflicts of interest The authors declare that they have no conflict of interest.

Research involving human participants and/or animals This article does not contain any studies with human participants or animals performed by any of the authors.

Informed consent This article is partially based on anonymized patient data.

References

1. Alterowitz R, Goldberg K (2008) Motion planning in medicine: optimization and simulation algorithms for image-guided procedures. Springer, Berlin
2. Beasley RA (2012) Medical robots: current systems and research directions. J Robot 2012:14
3. Burgner-Kahrs J, Rucker DC, Choset H (2015) Continuum robots for medical applications: a survey. IEEE Trans Robot 31(6):1261–1280
4. Caversaccio M, Gavaghan K, Wimmer W, Williamson T, Ansò J, Mantokoudis G, Gerber N, Rathgeb C, Feldmann A, Wagner F, Scheidegger O (2017) Robotic cochlear implantation: surgical procedure and first clinical experience. Acta Oto Laryngol 137(4):447–454
5. Cootes T, Taylor C, Cooper D, Graham J (1995) Active shape models-their training and application. Comput Vis Image Underst 61(1):38–59

6. Cowan NJ, Goldberg K, Chirikjian GS, Fichtinger G, Alterovitz R, Reed KB, Kallem V, Park W, Misra S, Okamura AM (2011) Robotic needle steering: design, modeling, planning, and image guidance. In: Rosen J, Hannaford B, Satava RM (eds) Surgical robotics: systems application and vision. Springer, US, Boston, MA, pp 557–582
7. Duindam V, Alterovitz R, Sastry S, Goldberg K (2008) Skrew-based motion planning for bevel-tip flexible needles in 3D environments with obstacles. In: IEEE international conference on robotics and automation, pp 2483–2488
8. Engh JA, Podnar G, Khoo SY, Riviere CN (2006) Flexible needle steering system for percutaneous access to deep zones of the brain. In: Proceedings of IEEE 32nd annual northeast bioengineering conference, pp 103–104
9. Fauser J, Stenin I, Kristin J, Klenzner T, Schipper J, Sakas G (2016) A software tool for planning and evaluation of non-linear trajectories for minimally invasive lateral skull base surgery. In: Tagungsb. der 15. Jahrestag. der Dtsch. Ges. f. Comput.- und Roboterass. Chirurgie e.V. (CURAC), pp 125–126
10. Fichera L, Dillon NP, Zhang D, Godage IS, Siebold MA, Hartley BI, Noble JH, Russell PT, Labadie RF, Webster RJ (2017) Through the eustachian tube and beyond: a new miniature robotic endoscope to see into the middle ear. IEEE Rob Autom Lett 2(3):1488–1494
11. Gammell JD, Srinivasa SS, Barfoot TD (2014) BIT*: Batch informed trees for optimal sampling-based planning via dynamic programming on implicit random geometric graphs. CoRR abs/1405.5848. arXiv:1405.5848
12. Gerber N, Bell B, Gavaghan K, Weisstanner C, Caversaccio M, Weber S (2014) Surgical planning tool for robotically assisted hearing aid implantation. Int J Comput Assist Radiol Surg 9(1):11–20
13. Hamze N, Collet P, Essert C (2017) Evolutionary approaches for surgical path planning: a quantitative study on deep brain stimulation. In: 2017 IEEE congress on evolutionary computation (CEC), pp 1087–1094
14. Hota S, Ghose D (2010) Optimal geometrical path in 3D with curvature constraint. In: 2010 IEEE/RSJ international conference on intelligent robots and systems, pp 113–118
15. Karaman S, Frazzoli E (2011) Sampling-based algorithms for optimal motion planning. Int J Robot Res 30(7):846–894
16. Kuffner JJ, LaValle SM (2000) RRT-connect: An efficient approach to single-query path planning. In: Proceedings 2000 ICRA. Millennium conference. IEEE international conference on robotics and automation. Symposia proceedings (Cat. No.00CH37065), vol 2, pp 995–1001
17. Labadie RF, Balachandran R, Noble JH, Blachon GS, Mitchell JE, Reda FA, Dawant BM, Fitzpatrick JM (2014) Minimally invasive image-guided cochlear implantation surgery: first report of clinical implementation. Laryngoscope 124(8):1915–1922
18. LaValle SM (2006) Planning algorithms. Cambridge Univercity Press, Cambridge
19. Liu F, Garriga-Casanovas A, Secoli R, y Baena FR (2016) Fast and adaptive fractal tree-based path planning for programmable bevel tip steerable needles. IEEE Robot Autom Lett 1(2):601–608
20. Noble JH, Majdani O, Labadie RF, Dawant B, Fitzpatrick JM (2010) Automatic determination of optimal linear drilling trajectories for cochlear access accounting for drill positioning error. Int J Med Robot 6(3):281–290
21. Patil S, Burgner J, Webster RJ, Alterovitz R (2014) Needle steering in 3-d via rapid replanning. IEEE Trans Robot 30(4):853–864
22. Pharpatara P, Hérissé B, Bestaoui Y (2017) 3-D trajectory planning of aerial vehicles using RRT*. IEEE Trans Control Syst Technol 25(3):1116–1123
23. Schulman J, Duan Y, Ho J, Lee A, Awwal I, Bradlow H, Pan J, Patil S, Goldberg K, Abbeel P (2014) Motion planning with sequential convex optimization and convex collision checking. Int J of Rob Res 33(9):1251–1270
24. Shkolnik A, Walter M, Tedrake R (2009) Reachability-guided sampling for planning under differential constraints. In: 2009 International conference on robotics and automation, pp 2859–2865
25. Stenin I, Hansen S, Becker M, Sakas G, Fellner D, Klenzner T, Schipper J (2014) Minimally invasive multi-port surgery of the lateral skull base. In: BioMed research international, vol 2014, p 7
26. Torres R, Kazmitcheff G, De Seta D, Ferrary E, Sterkers O, Nguyen Y (2017) Improvement of the insertion axis for cochlear implantation with a robot-based system. Eur Arch Oto Rhino Laryngol 274(2):715–721
27. Yang K, Gan SK, Huh J, Joo S (2014a) Optimal spline-based RRT path planning using probabilistic map. In: 2014 14th International conference on control, automation and systems (ICCAS 2014), pp 643–646
28. Yang K, Moon S, Yoo S, Kang J, Doh NL, Kim HB, Joo S (2014b) Spline-based RRT path planner for non-holonomic robots. J Intell Robot Syst 73(1):763–782
29. Yang L, Qi J, Jiang Z, Song D, Han J, Xiao J (2014c) Guiding attraction based random tree path planning under uncertainty: Dedicate for UAV. In: 2014 IEEE international conference on mechatronics and automation, pp 1182–1187